Vibrational Spectroscopy xxx (2012) xxx–xxx

Contents lists available at SciVerse ScienceDirect

Vibrational Spectroscopy

journal homepage: www.elsevier.com/locate/vibspec

From phonon confinement to phonon splitting in flat single nanostructures: A case of VO_2@V_2O_5 core–shell nano-ribbons

B.W. Mwakikunga[a,b,*], M. Maaza[c], K.T. Hillie[a,d], C.J. Arendse[e], T. Malwela[a], E. Sideras-Haddad[f]

[a] DST/CSIR National Centre for Nano-Structured Materials, PO Box 395, Pretoria 0001, South Africa
[b] Department of Physics and Biochemical Sciences, The Polytechnic-University of Malawi, Private Bag 303, Chichiri, Blantyre 0003, Malawi
[c] Materials Research Group, iThemba LABS, P O Box 722, Somerset West 7129, Cape Town, South Africa
[d] Physics Department, University of the Free State, P.O. 339, Bloemfontein, South Africa
[e] Department of Physics, University of the Western Cape, Private Bag X17, Bellville 7535, South Africa
[f] School of Physics, University of the Witwatersrand, Private Bag 3, Wits 2050, Johannesburg, South Africa

ARTICLE INFO

Article history:
Received 8 October 2011
Received in revised form 12 January 2012
Accepted 6 February 2012
Available online xxx

Keywords:
Vanadium oxides
Phonon confinement
Phonon splitting
Cations
Stoichiometry

ABSTRACT

Raman spectroscopy of the VO_x nano-ribbons is discussed in the framework of the Richter (1981) equation for optical phonon confinement (a) as modified for thin films by Fauchet and Campbell (1986), (b) as presented by Kim and co-workers for slabs, (c) as explained by Eklund's group for surface phonons and (d) our own modification based on the transformation from the spherical coordinates in the Richter equation to Cartesian coordinates; the latter being in keeping with the ribbon geometry. The change of coordinates also influences the profiles of the phonon dispersion curves. Phonon splitting is ascribed to the bi-layer and core–shell geometries of the ribbons and this is used to calculate the ratio of the V^{5+} to V^{4+} to the value of 0.54 ± 0.10. This is in perfect agreement with the $V^{5+}/V^{4+} \sim 54.60\%$ from X-ray photo-electron spectroscopy (XPS) measurements.

1. Introduction

Vanadium oxide (VO_x) is one of several transition-metal oxides that exhibit metal-to-insulator transition. The several main groups among the vanadium oxides are V_nO_{2n-1} (e.g. V_2O_3, V_7O_{13}) [1], V_nO_{2n+1} (e.g. V_2O_5, V_6O_{13} and V_3O_7) [2,3], V_nO_n (e.g. VO, V_2O_2) and V_nO_{2n} [3]. Among the V_nO_{2n} class, VO_2 is the most interesting because its transition temperature is close to room temperature ($T_c \sim 340$ K), and it displays $\sim 10^5$ decrease in resistivity as well as a large change in transparency in the infrared region. VO_2 is known to exist in four polymorphs (a) the most stable VO_2 rutile VO_2(R), (b) the metastable VO_2(M) with a slightly distorted rutile structure, (c) a tetragonal VO_2(A) and (d) the metastable VO_2(B) with a monoclinic structure [4].

VO_2 is thermo-chromic and can be used for window coatings to keep homes and buildings cool in summer and warm in winter, thereby saving electricity. VO_2 has been analysed by Raman spectroscopy [5]. This important material has been used in plasmonics [6] and ultrafast switches (since it shows a switching period of ~100 fs), holographic storage and recording industry [7] and protection from laser guided missiles in defence [8]. Raman spectra of the $CuO–V_2O_5–P_2O_5–CaO$ [9] glass system VO_x [10], VO_x supported on silica [13] have been presented. V_2O_5 finds applications in gas sensors [11], rechargeable vanadium batteries [11], vanadium superconducting SQUIDS [12] and hydrogen storage [14]. There have been some reports on Raman spectroscopy of VO_2 [5], and V_2O_5 [9,10,13,16] but, to our knowledge, none on the bi-layered $|V_2O_5|VO_2|$ or VO_2@V_2O_5 core–shell nano-ribbons of a combination of these phases and let alone the phenomenon of phonon confinement, phonon splitting and electronic transport on these structure. Also it has been difficult to determine phonon dispersion relations for the vanadium oxides by calculation [17] and let alone by the traditional neutron scattering method [18]. Due to vanadium's large scattering cross-section of neutrons, cans made from it are used in holding samples in typical neutron scattering experiments. So, it is difficult to find published data on phonon dispersion curves and their equations by this method in vanadium or its oxides. Here we attempt this task by Raman scattering through phonon confinement in ultrathin ribbons.

2. Background theory on phonon confinement and phonon splitting

Among the spatial correlation models, the phonon confinement model by Richter et al. [19] has been the most employed in studying

* Corresponding author. Tel.: +27 12 841 3874; fax: +27 12 841 2229.
E-mail address: bmwakikunga@csir.co.za (B.W. Mwakikunga).

0924-2031/$ – see front matter © 2012 Elsevier B.V. All rights reserved.
doi:10.1016/j.vibspec.2012.02.007

confined optical phonons in spherical structures due to spatial size effects. The so-called Richter equation is given by

$$I(\omega) = A_0 \int_{-\infty}^{\infty} \left[\frac{\left|C(0,\mathbf{q})\right|^2}{(\omega - \omega(\mathbf{q}))^2 + (\Gamma_0/2)^2} \right] d^3\mathbf{q} \quad (1)$$

where A_0 is a pre-factor to be determined from experiment, $|C(0,\mathbf{q})|^2$ are Fourier coefficients that depend on the size of the particle that scatters the light and the phonon momentum, ω is the phonon wave-number, $\omega(\mathbf{q})$ is the phonon dispersion relation for the material in the particle and Γ_0 is the full width at half maximum of the phonon peak of the bulk material. The $C(0,\mathbf{q})$ signifies that apart from the zone centre phonon of momentum $q_0 = 0$, there exists other phonons whose momentum $q \neq 0$ but centred at q_0. Campbell and Fauchet [20,21] suggested that the Fourier coefficient $|C(0,\mathbf{q})|^2\, d^3\mathbf{q}$ be given by $\exp(-\mathbf{q}^2 d^2/16\pi^2)\, d^3\mathbf{q}$. Their other achievement was their ability to extend the Richter model to other shapes of the micro-crystals such as what they called columnar (nano-rods, nano-wires) and also thin films. They argued that for thin films of thickness, τ, $|C(0,\mathbf{q})|^2$ should be equal to $\exp(-\mathbf{q}^2\tau^2/16\pi^2)|1 - \mathrm{erf}(i\tau/\sqrt{(32\pi)})|^2$.

Campbell and Fauchet admittedly saw very small significance in replacing the Gaussian with other size-distribution functions especially for spherical nano-crystals. Also the Fourier coefficients for thin films and columnar shapes make the Richter equation even more complicated in that one performs integration within another numerical integration with the second integration being complex in nature. A simpler approach to modifying the Richter equation to include other novel nano-crystal shapes has been considered. Following this argument, the Richter equation has been modified to account for the geometry of nano-wires by Piscanec et al. [22] and by Adu et al. [23,24] by changing the $d^3\mathbf{q}$ term for a sphere to $2\pi\mathbf{q}_\perp d\mathbf{q}_\perp$ for rods such that the Fourier coefficient is given by $2\pi\mathbf{q}_\perp \exp(-\mathbf{q}_\perp{}^2 d^2/16\pi^2)\, d\mathbf{q}_\perp$. Note that the constant $16\pi^2$ has been replaced with a scaling parameter α_{wire} that can be evaluated during the data fitting, as was performed by Mwakikunga et al. on WO_3 nanowires [25]. As for quantum dots, it is assumed that these structures are quasi-zero dimensional and hence all the atoms are surface atoms. Therefore, the d^3q term in Richter equation has been approximated to $d^3\mathbf{q} \propto \mathbf{q}^2 d\mathbf{q}$ [22]. Appropriately, this is equivalent to replacing $d^3\mathbf{q}$ by the momentum volume of $4\pi\mathbf{q}^2 d\mathbf{q}$ to give $|C(0,\mathbf{q})|^2 = 4\pi\mathbf{q}^2 \exp(-\mathbf{q}^2 d^2/a_{\mathrm{QD}}^2)\, d\mathbf{q}$ for quantum dots.

Slab-like nano-structures such as nano-belts, nano-platelets and nano-ribbons have phonon confinement only in one dimension. Dielectric continuum models developed as early as 1965 [26] and given in a review by Ruppin and Englman [27] have been extensively used to explain surface optical (SO) phonons as a function of dielectric constants of the material and the surrounding media. The SO phonon frequencies in this case are between transverse optical (TO) and longitudinal optical (LO) phonon frequencies given as [28]: $\omega_{\mathrm{SO}} = \sqrt{[(\{(m+1)/m\}\omega_{\mathrm{TO}}^2 + (\varepsilon_\infty/\varepsilon)\omega_{\mathrm{LO}}^2/(\{(m+1)/m\} + \varepsilon^{-1}\varepsilon_\infty)]}$. Such phonons have been reported to bear phonon dispersion relations given for symmetric (S) and anti-symmetric (AS) modes respectively as: $\omega_{\mathrm{SO}}^2(q)_{\mathrm{S}} = \omega_{\mathrm{TO}}^2[(\varepsilon_0 \tanh(q_i L_i/2) + \varepsilon_{\mathrm{m}})/(\varepsilon_\infty \tanh(q_i L_i/2) + \varepsilon_{\mathrm{m}})]$ and $\omega_{\mathrm{SO}}^2(q)_{\mathrm{AS}} = \omega_{\mathrm{TO}}^2[(\varepsilon_0 \coth(q_i L_i/2) + \varepsilon_{\mathrm{m}})/(\varepsilon_\infty \coth(q_i L_i/2) + \varepsilon_{\mathrm{m}})]$.

SO phonons in cylindrical nanowires were noticed in core–shell GaP@GaN nanowires [29] and explained by Gupta et al. [30] and by Xiong et al. [31,32] in rectangular cross-section nanowires of ZnS. Recently, SO phonons from 50-nm thick GaN nano-ribbons were reported [33]. Although, Xiong et al. [34] has reviewed SO phonon frequency to relate SO phonons to the particle size and shape, this has been done on ribbons no thinner than 20 nm and the theory employed has been up to the traditional dielectric continuum models already mentioned. Around this thickness, the Richter phonon confinement model is pushed to its limits and therefore such ribbons can be regarded as bulk [35,36]. Also, SO frequencies falling between TO and LO cannot explain new phonons having frequencies outside this range, but have often been explained by TO-splitting and LO-splitting. This is now a new phenomenon.

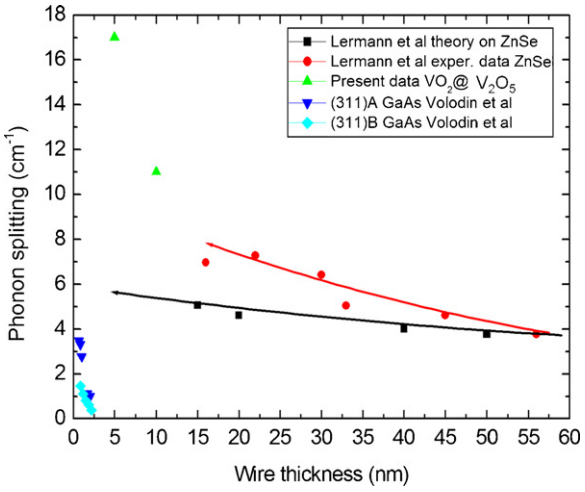

Fig. 1. Lermann's theory of phonon splitting based on stress studies could fit experimental data only if the wire width was not less than about 70 nm.
Adapted from Ref. [37]

Lermann et al. [37] have previously derived a theory based on stress in multilayered ZnSe quantum wires to relate the LO-splitting range to the wire width, but their calculated splitting matched experimental data only down to about 70 nm of wire width. The theory failed to fit experimental data below 50 nm as re-produced in Fig. 1. Kim and Jang [38] however were some of the earliest in employing a quantum-mechanics-based Richter equation to explain confinement in isolated slabs but not TO-splitting or LO-splitting. Since they did not notice LO- and/or TO-splitting due to SO phonons in their Raman spectra, they supposed that the Fourier coefficient must generally be given by $f(\mathbf{q})\exp(-\mathbf{q}^2 d^2/\alpha_{\mathrm{slab}})d\mathbf{q}$ where $f(\mathbf{q}) = 1$ for slabs. However, changing only the weighting function without changing the phonon dispersion relations can only help adjust the amplitude of the confined phonons with the aid of α_{slab} but without the explanation of the phonon splitting.

In this paper, we suggest re-starting from Richter et al. optical confinement model and following the simpler approach of simply changing not only the dimensionality of the $d^3\boldsymbol{q}$ momentum volume in the exponential function but also manipulating the dimensionality of the phonon dispersion relations to suit the nano-ribbon geometry in the present case.

This way, we have a new proposed model that would easily explain the phonon splitting in nano-ribbon and other flat structures.

3. New dimensionality in OPC that suits the ribbon geometry

Let us consider the following schematics of Fig. 1(a) and (b) of a ribbon interacting with a laser beam in a typical Raman spectroscopy set-up. In performing Raman spectroscopy on ribbons whose typical length (L_x), width (L_y) and thickness (L_z) are about 1 μm × 400 nm × 10 nm as shown by our AFM results presented in the forthcoming sections, one expects that confinement of optical phonons ought to be only in one dimension, that is, the z direction which denotes the thickness of the ribbon as illustrated in the inset of Fig. 1(a). We start from the Fourier coefficients and dispersion

Please cite this article in press as: B.W. Mwakikunga, et al., From phonon confinement to phonon splitting in flat single nanostructures: A case of VO_2@V_2O_5 core–shell nano-ribbons, Vib. Spectrosc. (2012), doi:10.1016/j.vibspec.2012.02.007

relations respectively as given in spherical co-ordinates by Arora et al.'s review papers [35,36] and a similar exponential function in Zhu et al. [39], to mention a few, as follows:

$$\left|C(0,\mathbf{q})\right| = \exp\left(-\frac{d^2\mathbf{q}^2}{2\alpha}\right) = \exp\left(-\frac{4r^2\mathbf{q}^2}{2\alpha}\right) = \exp\left(-\frac{2r^2\mathbf{q}^2}{\alpha}\right) \tag{2a}$$

$$\omega(\mathbf{q}) = \omega_0 \pm \Delta\omega \sin^2\left(\frac{a\mathbf{q}}{\mathbf{2}}\right) \tag{2b}$$

where $d = 2r$ (r being the radius) is the diameter of a sphere. Changing from the spherical co-ordinates, in which Eqs. (2a) and (2b) are written, to Cartesian coordinates. Bearing in mind that $\mathbf{r} = L_x\mathbf{i} + L_y\mathbf{j} + L_z\mathbf{k}$, $\boldsymbol{q} = q_x\mathbf{i} + q_y\mathbf{j} + q_z\mathbf{k}$, $\boldsymbol{\delta} = a\mathbf{i} + b\mathbf{j} + c\mathbf{k}$, the magnitudes $|\mathbf{r}|^2 = r^2 = L_x^2 + L_y^2 + L_z^2$, $|\mathbf{q}|^2 = q^2 = q_x^2 + q_y^2 + q_z^2$ and $|\boldsymbol{\delta}|^2 = \delta^2 = a^2 + b^2 + c^2$. Their multiplication can either be vector ($\mathbf{r}\times\mathbf{q}$), ($\boldsymbol{\delta}\times\mathbf{q}$) or scalar ($\mathbf{r}\cdot\mathbf{q}$), ($\boldsymbol{\delta}\cdot\mathbf{q}$) products. The reader may recall that the magnitudes $|\mathbf{r}\times\mathbf{q}| = |\mathbf{r}|\cdot|\mathbf{q}|\sin\theta$ and $|\mathbf{r}\cdot\mathbf{q}| = |\mathbf{r}|\cdot|\mathbf{q}|\cos\theta$ and so on, where θ is the angle between $\mathbf{r}$ and $\mathbf{q}$ for instance. Choosing scalar products in the spirit of the Richter's phonon confinement model (vector products will be beyond the present discussion), one gets $|\mathbf{r}\times\mathbf{q}|^2 = |\mathbf{r}|^2 \times |\mathbf{q}|^2\cos^2\theta = r^2\cdot q^2\cdot\cos^2\theta = (L_x^2 + L_y^2 + L_z^2)(q_x^2 + q_y^2 + q_z^2)\cdot\cos^2\theta$ and $|\boldsymbol{\delta}.\mathbf{q}| = |\boldsymbol{\delta}|\cdot|\mathbf{q}|\cdot\cos\theta = d\cdot q\cdot\cos\theta = \sqrt{(a^2+b^2+c^2)}\sqrt{(q_x^2+q_y^2+q_z^2)}\cdot\cos\theta$. Expanding these components, one finds that perpendicular components ($\theta = \pi/2$) are of non-effect and they vanish. Only parallel components ($\theta = 0$) are important.

During the Raman spectroscopy experiment, the exciting laser is directed along the z-axis of the ribbon. The preferential growth direction of the ribbon is along the c-axis parallel to the glass substrate as was also found by Ramana et al. [16], which has the longest parameter of about 12.3 Å in VO_2, whereas the other parameters $a = 3.4$ Å and $b = 4.3$ Å. These lattice parameter values are similar to those in V_2O_5. From how our ribbons grow, it can then be seen that the z-axis corresponds to lattice parameter a (the confining direction), the y-axis to the lattice parameter b and the x-axis to lattice parameter c. This means the x and y directions describe the surface of the ribbon which is perpendicular to the laser beam direction. Therefore one gets for the Fourier coefficients and dispersion coefficients for the ribbon geometry as follows:

$$|C(0,\mathbf{q})| = \exp\left(-\frac{2r^2\mathbf{q}^2}{\alpha}\right) = \exp\left(-\frac{2(L_x^2q_x^2 + L_y^2q_y^2 + L_z^2q_z^2)}{\alpha}\right) \tag{3a}$$

$$\omega(q) = \omega_0 \pm \Delta\omega \sin^2\left(\tfrac{1}{2}(cq_x + bq_y + aq_z)\right) \tag{3b}$$

It is now possible to re-write the Richter et al. equation (Eq. (1)), which is in spherical co-ordinates, to an equation that is in Cartesian ones in keeping with the geometry of nano-ribbons illustrated in inset of Fig. 1(a). We also consider the contribution to the line-shape from ribbons of varying thickness with a distribution $\rho(L_z)$ as follows:

$$I(\omega) = A_0\int_0^\infty \rho(L_z)\,dL_z \times \int_0^{Q_z}\int_0^{Q_y}\int_0^{Q_x} \frac{\exp(-2(L_x^2q_x^2 + L_y^2q_y^2 + L_z^2q_z^2)/\alpha)}{[\omega - \omega_0 \mp \Delta\omega\sin^2((1/2)(cq_x + bq_y + aq_z))] + (1/4)\Gamma_0^2}\,dq_x\,dq_y\,dq_z \tag{4}$$

Here A_0 is a prefactor, a, b and c are lattice parameters of the unit cell and the limits of integration, Q_x, Q_y and Q_z, in all direction are up to the first Brillouin zone but can extend to ∞. Expanding this multiple integration leads to:

$$I(\omega) = A_0\int_0^\infty \rho(L_z)\,dL_z \times \int_0^{Q_z}\int_0^{Q_y}\int_0^{Q_x} \frac{\exp(-L_x^2q_x^2/\alpha)\exp(-L_y^2q_y^2/\alpha)\exp(-L_x^2q_z^2/\alpha)}{[\omega - \omega_0 \mp \Delta\omega\sin^2((1/2)(cq_x + bq_y + aq_z))] + (1/4)\Gamma_0^2}\,dq_x\,dq_y\,dq_z \tag{5}$$

and grouping the confinement term, q_z, away from the non-confinement terms – q_x and q_y – we obtain an equation that is suitable for Raman scattering in thin layers such as ribbons, sheets and belts as follows:

$$I(\omega) = A_0\int_0^\infty\int_0^\infty \exp\left(-\frac{2L_x^2q_x^2}{\alpha}\right) \times \exp\left(-\frac{2L_y^2q_y^2}{\alpha}\right) dq_x\,dq_y \int_0^\infty \rho(L_z)\,dL_z \times \int_0^{Q_z} \frac{\exp(-2(L_z^2q_z^2)/\alpha)}{[\omega - \omega_0 \mp \Delta\omega\sin^2(Q_{surf} + (1/2)aq_z)]^2 + (1/4)\Gamma_0^2}\,dq_z,$$
$$Q_{surf} = \frac{1}{2}(bq_y + cq_x) \tag{6}$$

The double integration describes the magnitude (amplitude) of the non-confined vibrational modes in the q_x–q_y momentum surface and hence the ribbon's (x–y) surface. Note that, as expected, the profiles of the (x–y) phonon spectra are perfect Gaussians. However, the numerical integration with respect to q_z is the only component that describes the asymmetrical broadening in the Raman spectrum. By definition in Eq. (6), Q_{surf} is an angular factor that scales the Raman shift of the surface phonons and the consequent observed splitting. This factor is dictated by lattice parameters in the non-confining directions. The double integration can be a constant, A_0', for a given ribbon shape and material. A_0' scales the intensity of the surface phonons. This means there are two factors, A_0' and Q_{surf}, which can be adjusted depending on shape and the type of material to fit the experimental line-shape of the Raman spectrum of a slab-like material. Hence the whole equation can be written as:

$$I(\omega) = A_0'\int_0^\infty \rho(L_z)\,dL_z \times \int_0^{Q_z} \times \frac{\exp(-2(L_z^2q_z^2)/\alpha)}{[\omega - \omega_0 \mp \Delta\omega\,\sin^2(Q_{surf} + (1/2)aq_z)]^2 + (1/4)\Gamma_0^2}\,dq_z \tag{7}$$

This equation not only fits asymmetrically broadened peaks due to phonon confinement, which is also due to ribbon thickness effects, but also explains the emergence of at least one new phonon peak of momentum $\pm\Delta\omega\sin^2(Q_{surf} + aq_z)$ above (+) or below (−) the zone centre ω_0.This is dictated by the phonon dispersion relations both in the confining dimension, z, and on the surface, x–y. This equation would therefore link the ribbon thickness L_x, L_y, L_z to the nature of surface phonons and the phenomena of TO-splitting and LO-splitting in such flat structures.

We will initially show how Eq. (7) explains the phonon dynamics – from phonon confinement in nanostructures to phonon splitting. The latter phenomenon is enhanced especially in flat structures. Fitting of this equation to experimental data follows in Section 5.

Please cite this article in press as: B.W. Mwakikunga, et al., From phonon confinement to phonon splitting in flat single nanostructures: A case of VO_2@V_2O_5 core–shell nano-ribbons, Vib. Spectrosc. (2012), doi:10.1016/j.vibspec.2012.02.007

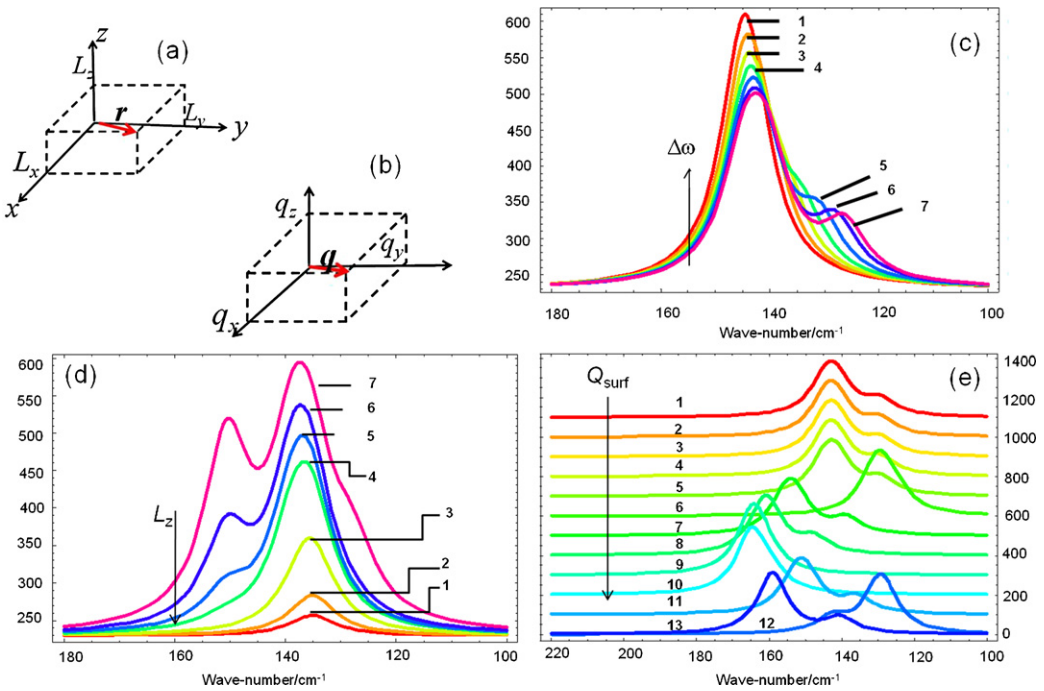

Fig. 2. Geometrical consideration of the ribbons (a) $\boldsymbol{r}$-space and (b) $\boldsymbol{q}$-space. How the lineshapes of Eq. (7) look like (c) when, at a constant $Q_{surf} = 2.9 \times 10^{-4}$ rads and $L_z = 7$ nm, $\Delta\omega$ is increased from 1 to 7 of respective values in cm^{-1} of +2, +6, +10, +14, +18, +22 and +24 (d) when the ribbon thickness, L_z, is decreased, at a constant $Q_{surf} = 2.9 \times 10^{-4}$ rads and $\Delta\omega = +20\,cm^{-1}$, from 1 to 7 of respective values in nm of 100, 50, 20, 10, 8, 6 and 4 and (e) when, at a constant $L_z = 7$ nm and $\Delta\omega = +20\,cm^{-1}$, the value of Q_{surf} is increased from 1, 2, 3, 4, 5, 6, 7, 8, 9, 10, 11, 12 to 13 with the respective values in rads^2 of $\sim 10^{-6}$, 10^{-5}, 10^{-4}, 10^{-3}, 10^{-2}, 10^{-1}, 10^{0}, 10^{2}, 10^{3}, 10^{4}, 10^{5}, 10^{6}, 10^{7} [*Note*: the lineshapes in (e) are stacked for clarity].

Fig. 2(c–e) show how the Raman lineshapes of Eq. (7) appear when some of its variables are changed – how the degree of splitting (ω_0–ω_{SO}) is affected by ribbon thickness L_z, dispersion parameter $\Delta\omega$ and surface component of the phonon momentum, Q_{surf}. These figures depict Eq. (7) lineshape (c) when, at a constant $Q_{surf} = 2.9 \times 10^{-4}$ rads^2 and $L_z = 7$ nm, $\Delta\omega$ is increased from 1 to 7 of respective values in cm^{-1} of +2, +6, +10, +14, +18, +22 and +24 (d) when the ribbon thickness, L_z, is decreased, at a constant $Q_{surf} = 2.9 \times 10^{-4}$ rads^2 and $\Delta\omega = +20\,cm^{-1}$, from 1 to7 of respective values in nm of 100, 50, 20, 10, 8, 6 and 4 and (e) when, at a constant $L_z = 7$ nm and $\Delta\omega = +20\,cm^{-1}$, the value of Q_{surf} is increased from 1, 2, 3, 4, 5, 6, 7, 8, 9, 10, 11, 12 to 13 with the respective values in rads^2 of $\sim 10^{-6}$, 10^{-5}, 10^{-4}, 10^{-3}, 10^{-2}, 10^{-1}, 10^{0}, 10^{2}, 10^{3}, 10^{4}, 10^{5}, 10^{6}, 10^{7}.

In Fig. 2(c), increasing the dispersion parameter $\Delta\omega$ directly increases the degree of splitting while decreasing the intensity of the individual phonons. In (d), L_z at 100 nm and 50 nm show Gaussian lineshapes centred at 145 cm^{-1}.

Asymmetry shows up as L_z approaches 20 nm. Beyond 20 nm, one begins to see a new phonon band (around 128 cm^{-1}) below the zone centre wavenumber and this continues to intensify as L_z goes down to 4 nm. One notes that L_z does not affect the degree of splitting but the intensity of the split phonons increases as L_z decreases. Below $L_z = 4$ nm, the lineshape shows an extra shoulder above the zone centre frequency.

In Fig. 2(e), Q_{surf} affects both the intensity of the individual split phonons and, as expected, the degree of splitting fluctuates sinusoidally as this parameter is changed. Since $\sin^2(Q_{surf} + aq_z)$ fluctuates between +1 and −1, when $Q_{surf} + aq_z = (n-1)\pi$ where $n = 1, 2, 3, \ldots$, the sine value is zero for every n and therefore the lineshape is only dictated by the value of $\Delta\omega$. This is what happens when $10^{-6} > Q_{surf} > 10^{-2}$. However, when $Q_{surf} + aq_z = (1 + 2(n-1))\pi/2$, the lineshape has the split phonon either below (+1) or above (−1) the zone centre. This is what happens when $Q_{surf} > 10^{-2}$. At this point one sees instability in the position of the zone centre phonon peak as well as the split phonon peak. The instability is oscillatory whose frequency increases as Q_{surf}. Proper understanding of how these parameters affect the lineshape is useful during the fitting process in order to obtain the optimum values of Q_{surf}, L_z and $\Delta\omega$ for a given Raman spectral data set. This is dealt with in the forthcoming sections.

4. Ribbon sample production and characterisation techniques

The VO_2 nanoribbons were produced by ultrasonic spray pyrolysis (USP). The experimental setup for USP was fully described [40–42]. Morphology studies were carried out using a LEO 1525 field emission gun scanning electron microscope (FEG-SEM) operated at 3–20 kV, equipped with energy dispersive X-ray spectroscopy (EDS). In order to avoid charging effects during SEM analysis, the samples were made conductive by carbon coating. Structural studies were done using a Panalytical Xpert powder diffractometer equipped with a Cu K_α wavelength of 0.154184 nm. Transmission electron microscopy (HRTEM) was carried on a CM 200 Jeol microscope.

AFM topography examinations were carried out with the Multimode AFM NanoScope Version (R) IV (VEECO instrument) using a 0.5–2 Ω cm phosphorous (n) doped Si tip with a radius of curvature of 10 nm and the aspect ratio of 1:1. An aliquot of VO_2 nano-ribbons powder was suspended in ethanol and a drop of the sonicated ribbons was placed onto a clean Si (1 1 1) surface. Imaging was done in tapping mode (TM) and varying the scan rates and magnifications. In order to determine the thickness of the ribbon, AFM measurements were coupled with SEM by tilting the stage in SEM to an angle ϕ to the electron beam. This exposed the third dimension (tilted thickness, τ_z') of the ribbons. The actual thickness, τ_z, was calculated as $\tau_z = t_z' \cos f$. A size distribution was then quickly determined.

Raman spectroscopy was conducted using a Jobin-Yvon T64000 Raman spectrograph with a 514.5 nm line from an argon ion laser.

Please cite this article in press as: B.W. Mwakikunga, et al., From phonon confinement to phonon splitting in flat single nanostructures: A case of VO_2@V_2O_5 core–shell nano-ribbons, Vib. Spectrosc. (2012), doi:10.1016/j.vibspec.2012.02.007

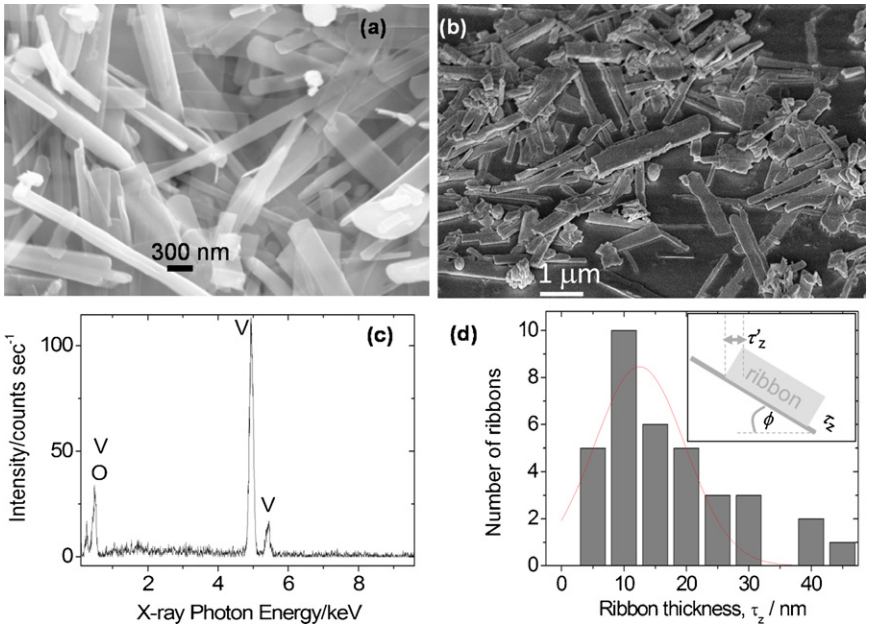

Fig. 3. (a) SEM micrograph of VO_2 nano-ribbons, (b) tilted at $\phi = 54^\circ$, (c) an EDS spectrum showing the V and O peaks on a carbon adhesive tape substrate and (d) size (thickness) distribution histogram (thickness determined from $\tau_z = \tau'_z/\sin\phi$ as illustrated in the inset of (d)).

The power of the laser at the sample was small enough (0.384 mW) in order to minimise localised heating of the sample. The T64000 was operated in single spectrograph mode, with the 1800 lines/mm grating and a 100× objective on the microscope. Fitting of Eq. (7) to the Raman spectral data is accomplished by "Nonlinear Fit" command and a numerical integration "NIntegrate" algorithm in Mathematica.

5. Results and discussion

Nano-ribbons illustrated in the SEM in Fig. 3(a) are seen at the following synthesis parameters: (1) at highest flow rate of 18 sccm of argon of the NH_4VO_3 precursor, (2) the substrate of borosilicate glass, (3) positioned at a region in the furnace where the substrate temperature was ~300 °C and (4) the furnace temperature of 700 °C

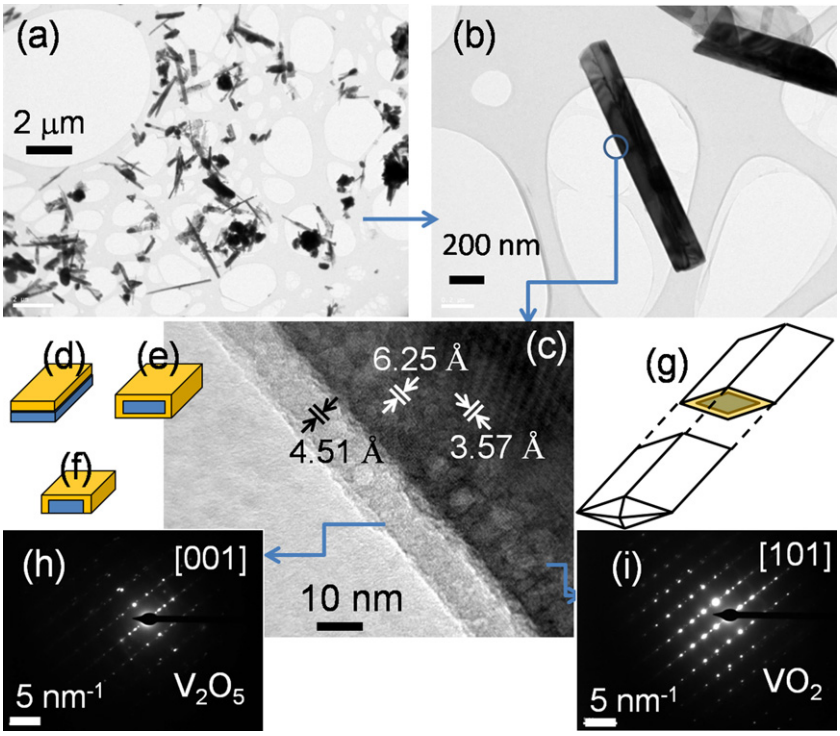

Fig. 4. Transmission electron microscopy: (a) low resolution image, (b) low resolution on a single ribbon, (c) higher resolution on the edge of ribbon revealed bi-layered structure: V_2O_5 and VO_2 and in some ribbons a core–shell structure. (d) and (e) are SAED patterns for V_2O_5 and VO_2 regions respectively, (f) AFM height image of a single VO_2 nano-ribbon. The profile (g) shows that the VO_2 ribbon is typically 10 nm thick.

Please cite this article in press as: B.W. Mwakikunga, et al., From phonon confinement to phonon splitting in flat single nanostructures: A case of VO_2@V_2O_5 core–shell nano-ribbons, Vib. Spectrosc. (2012), doi:10.1016/j.vibspec.2012.02.007

in the central zone. Note the EDS spectra shows only V and O peaks with some C peak from the carbon tape.

XRD results (not shown) indicated that our VO_x is a mixture of many phases, but the most predominant are the V_2O_5, VO_2(M) and VO_2(B). Low magnification TEM, Fig. 4(a), shows that the ribbons' yield is high and of considerable variety. Higher magnification on the edge of one ribbon of Fig. 4(b) showed that the ribbon [Fig. 4(c)] has two main layers: an outer (shell) layer of oxygen-rich VO_x with one lattice spacing measured as 4.511 Å indexed to the parameters of V_2O_5 [c = 4.383 Å] and an inner (core) with lattice spacing values of 6.2517 Å and 3.5712 Å indexed to twinned phases of stoichiometric VO_2(M) and VO_2(B). Fig. 4(d–g) is illustrations of the variety of morphologies of these ribbons from bi-layers of $|V_2O_5|VO_2|$ to $VO_2@V_2O_5$ core–shell structures. Selected area electron diffraction (SAED) patterns for the two regions, in Fig. 4(c) show high crystallinity from well-defined interference spots in the SAED patterns ((h) and (i)). Energy dispersive X-ray spectroscopy (EDS) spectra (not shown) qualitatively confirmed the comparative oxygen content in the two layers; the outer layer was oxygen-rich showing a stoichiometry close to that of V_2O_5 whereas the core showed presence of VO_2. Quantitative XPS results confirming the qualitative EDS findings will be discussed in the sections to follow.

Fig. 4(f) shows the 1.1 μm × 1.1 μm AFM height topography of an isolated ribbon. The profile (g) clearly shows that the ribbon in the image has a thickness of 10 nm. The other dimensions of width and length are 400 nm and 1000 nm, respectively.

5.1. Phonon splitting and phonon dispersion relation for the V_2O_5/VO_2 composite ribbons

Fig. 5 presents the Raman spectra of the V_2O_5/VO_2(B) nano-ribbon. It is well known that some lines of V_2O_5 are very close in position to the lines of VO_2 – for example, 141, 196, 302, and 403 cm^{-1} lines which are usually assigned to V_2O_5 – are present in Raman spectra of VO_2 at the temperatures above its phase transition [5]. VO_2(M) below the transition temperature has prominent phonon peaks [5–10] at ~145 cm^{-1} and 617 cm^{-1}. Our V_2O_5/VO_2 (B) belts show a very prominent phonon peak at around 146 cm^{-1} but none at 617 cm^{-1}. The absence at 617 cm^{-1} could be due to the V_2O_5 layer masking the VO_2. The transverse optical (TO) and longitudinal optical (LO) phonon assignments are indicated in Fig. 5(a). A close-up of the main 141–145 cm^{-1} phonons in Fig. 5(b) shows asymmetrical broadening of the 141 cm^{-1} phonon line-shape. Eq. (7) has been fitted to our Raman spectroscopy data in order to obtain unknown parameters in the dispersion relations – $\Delta\omega$ and Q_{surf} – the exponential weighting function, α_{ribbon}, and the pre-factor A_0'. This parameter extraction exercise is conceptionally justified from the previous studies [39], where the phonon confinement model (Eq. (1)) was employed, given a precise particle size, to obtain parameters in the theoretical phonon dispersion relations of anatase TiO_2 quantum dots. From the fitting of Eq. (7) to the Raman spectral data obtained on spot 1 (the edge of a typical ribbon), the phonon dispersion relations in the range 120–150 cm^{-1} for VO_2/V_2O_5 for the first time become:

$$\omega(q) \approx 141 - 3\sin^2\left(Q_{surf} + \tfrac{1}{2}aq\right) \quad (8)$$

$Q_{surf} = 4.6 \times 10^{-6}$ rad, a = 4 Å and ribbon thickness, L_z, of 8.2 ± 3.3 nm, Γ = 10 cm^{-1}, α = 160.

Also Fig. 5(b) reveals a split of the V_2O_5's 141 cm^{-1} phonon into two – 126 cm^{-1} and 145 cm^{-1} – when the Raman scattering is performed on spot 2 (the middle of the bilayer). The split could be due to a number of reasons: (1) changes in the phonon dispersion parameter, $\Delta\omega$, as seen from the current theory, which could be due to the effect of the V_2O_5 and VO_2 composite; (2) enhancement of the split phonon due to decrease in ribbon thickness on spot 2; (3) the enhancement of surface components of the phonons, Q_{surf}, at this scale; and (4) phonon confinement due to ribbon thickness, L_z generates other modes of vibrations.

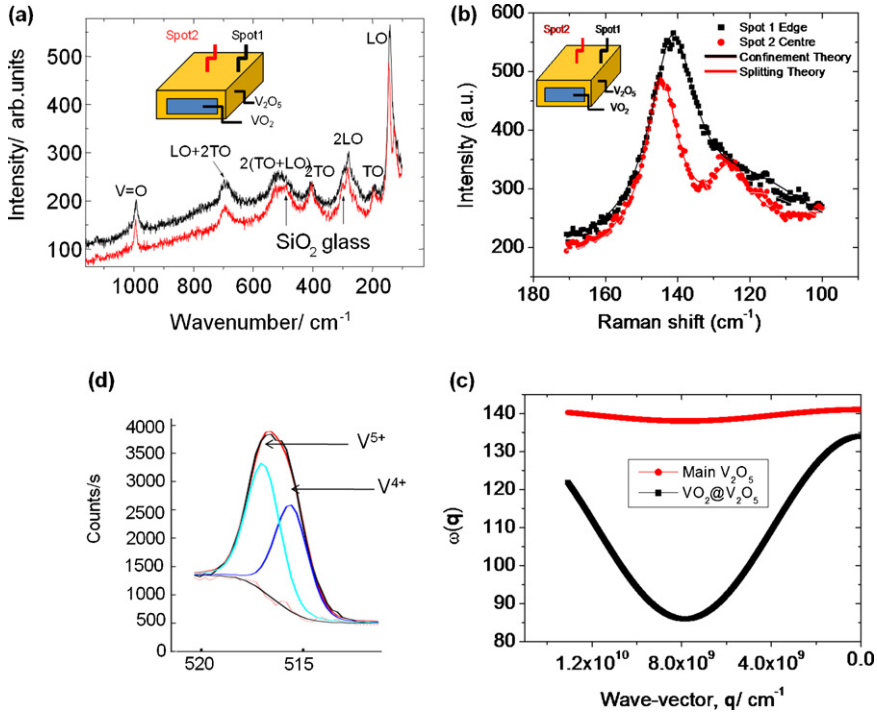

Fig. 5. (a) Raman spectra for two spots on the V_2O_5/VO_2 nano-ribbons with the possible assignments. (b) A close-up of the 141–145 cm^{-1} phonon region revealing a 141 cm^{-1} TO-splitting into two phonons – 126 cm^{-1} (V_2O_5) and 145 cm^{-1} (VO_2). (c) A plot of phonon dispersion relations from the fitting session given in Eqs. (8) and (9) for V_2O_5 and $VO_2@V_2O_5$ composite respectively. (d) A detailed XPS spectrum of V showing the distribution of the V^{4+} and V^{5+} cations.

Please cite this article in press as: B.W. Mwakikunga, et al., From phonon confinement to phonon splitting in flat single nanostructures: A case of $VO_2@V_2O_5$ core–shell nano-ribbons, Vib. Spectrosc. (2012), doi:10.1016/j.vibspec.2012.02.007

The fitting of Eq. (7) to this latter data yield the following phonon dispersion relation for VO_2/V_2O_5 composite as follows:

$$\omega(q)_{\text{splitting}} \approx 134 - 48\sin^2\left(Q_{\text{surf}} + \tfrac{1}{2}aq\right) \quad (9)$$

where Q_{surf} increases to 7.64×10^{-2} rad. From the definition of Q_{surf} in Eq. (6) and assuming that $q_x \sim q_y \sim q_{\text{surf}}$, we find that $q_{\text{surf}} < 5\times10^3\,\text{cm}^{-1}$ for the case of pure phonon confinement without splitting and $5\times10^3\,\text{cm}^{-1} < q_{\text{surf}} < 1\times10^8\,\text{cm}^{-1}$ for steady phonon splitting whereas $q_{\text{surf}} > 1\times10^8\,\text{cm}^{-1}$ for oscillatory phonon splitting in the V_2O_5@VO_2 core–shell geometry.

From the closeness of the Raman lines of the VO_2 and V_2O_5, the 145 cm^{-1} peak is due to both the V^{4+} and V^{5+} from VO_2 and V_2O_5 respectively whereas the 126 cm^{-1} split shoulder is from the V^{5+} valence state of V_2O_5 alone. The speculation about the latter 126 cm^{-1} phonon assignment has been validated by an ab initio Raman spectrum calculation from density functional perturbation theory on V_2O_5 by Zhou et al. [11] and Clauws et al. [14] who assigned its phonon peak at 123 cm^{-1} to B_{1u}(IR) of V_2O_5. Also, experimental results on aqueous VO_x by Gao et al. [15] revealed a sharp phonon peak at 129 cm^{-1} in these V_2O_5 based materials. Therefore, the 126 cm^{-1} phonon wave-number in the present results is likely to be due to the V^{5+} state in our ribbons. This phonon splitting can help us indirectly to quantify the ratio V^{5+}/V^{4+} thus:

$$\frac{N(V_2O_5)}{N(VO_2)} = \frac{V^{5+}}{V^{4+}} = \frac{\int_{123\,\text{cm}^{-1}} I(\omega)\,d\omega}{\int_{145\,\text{cm}^{-1}} I(\omega)\,d\omega} = 0.54 \pm 0.1 \quad (10)$$

We can also explain this splitting as due to surface phonons as the surface to volume ratio increases with decreasing ribbon thickness. The V^{5+}/V^{4+} ratio as determined from the phonon splitting in Raman spectra by dividing the area under the 126 cm^{-1} peak to that under the 145 cm^{-1} peak, which came to be 0.54 ± 0.1 as shown in Eq. (10), has been corroborated by XPS results from the same sample which indicate the V_2O_5/VO_2 ratio is about 54.6%. This is a remarkable agreement that suggests that rich information hides in split phonons displayed by Raman spectra of materials.

6. Conclusion

We have presented ultra-thin ribbons of VO_2 of B phase and other phases of VO_2 especially those of monoclinic M and B phases with a shell of V_2O_5 as determined by TEM and XRD. Raman spectroscopy shows optical phonon confinement only in the thickness dimension of typically 10 nm. For thinner ribbons, phonon splitting is evidence of two main phases – VO_2 and V_2O_5. In order to explain the spectra, we have derived a new phonon confinement model suited for geometrically flat structures by changing from spherical coordinates in the Richter et al. original phonon confinement model to Cartesian co-ordinates. This was necessary to explain the new features in Raman spectra of the nanoribbons as a result of splitting of phonons as well as obtain the scarce phonon dispersion relations for the V_2O_5 and VO_2 systems. We have also shown that in principle that Raman spectroscopy is as good as XPS when employed in the quantitative analysis of stoichiometry in compound as well as determining the quantities available in a sample of various phases.

Acknowledgements

Ms. Alison Tuling of the Department of Mechanical Engineering at the University of Pretoria is acknowledged for the TEM images, the National Metrology Institute of South Africa for the XRD and SEM. The first author wishes to thank the Japanese Government and the World Bank in Washington for the financial support drawn from the Joint Japan/World Bank Graduate Scholarship Programme (JJWBGSP).

References

[1] F.J. Morin, Phys. Rev. Lett. 3 (1959) 34.
[2] S. Mathur, T. Ruegamer, I. Grobelsek, Chem. Vapor Deposition 13 (2007) 42.
[3] M. Occhiuzzi, D. Cordischi, R. Dragone, J. Solid State Chem. 178 (2005) 1551.
[4] A. Haras, M. Witko, D.R. Salahub, K. Hermann, R. Tokarz, Surf. Sci. 491 (2001) 77.
[5] G.I. Petrov, V.V. Yakovlev, J. Squier, Appl. Phys. Lett. 81 (2002) 1023.
[6] D. Vernardou, M.E. Pemble, D.W. Sheel, Surf. Coat. Technol. 188–189 (2004) 250–254.
[7] M. Pan, J. Liu, H. Zhong, S. Wang, Z-F. Li, X. Chen, W. Lu, J. Crystal Growth 268 (2004) 178–183.
[8] T.D. Manning, I. Parkin, J. Mater. Chem. 14 (2004) 2554–2559.
[9] N. Vedeanu, O. Cozar, I. Ardelean, B. Lendl, D.A. Magdas, Vib. Spectrosc. 48 (2008) 259–262.
[10] A. Bouzidi, N. Benramdane, S. Bresson, C. Mathieu, R. Desfeux, M. El Marssi, Vib. Spectrosc. 57 (2011) 182–186.
[11] B. Zhou, D. He, J. Raman Spectrosc. 39 (2008) 1475.
[12] G.T. Went, S. Ted Oyama, A.T. Bell, J. Phys. Chem. 94 (1990) 4240–4246.
[13] D.E. Keller, T. Visser, F. Soulimani, D.C. Koningsberger, B.M. Weckhuysen, Vib. Spectrosc. 43 (2007) 140–151.
[14] P. Clauws, J. Broeckx, J. Vennik, Phys. Stat. Sol. B 131 (1985) 459.
[15] X. Gao, S.R. Bare, B.M. Weckhuysen, I.E. Wachs, J. Phys. Chem. B 102 (1998) 10842–10852.
[16] C.V. Ramana, O.M. Hussain, B. Srinivasulu Naidu, P.J. Reddy, Thin Solid Films 305 (1997) 219–226.
[17] F. Gervais, W. Kress, Phys. Rev. B 31 (1985) 4809–4814.
[18] A.K. Cheetham, C.N.R. Rao, Acta Cryst. 32 (1976) 1579.
[19] H. Richter, Z.P. Wang, L. Ley, Solid State Commun. 39 (1981) 625.
[20] P.M. Fauchet, I.H. Campbell, C.R. Solid State Mater. 14 (1988) 79.
[21] I.H. Campbell, P.M. Fauchet, Solid State Commun. 58 (1986) 739.
[22] S. Piscanec, M. Cantoro, A.C. Ferrari, J.A. Zapien, Y. Lifshitz, S.T. Lee, S. Hoffmann, J. Robertson, Phys. Rev. B 68 (2003) 241312R.
[23] K.W. Adu, H.R. Gutierrez, U.J. Kim, G.U. Sumanasekera, P.C. Eklund, Nano Lett. 5 (2005) 400.
[24] K.W. Adu, Q. Xiong, H.R. Gutierrez, G. Chen, P.C. Eklund, Appl. Phys. A 85 (2006) 287–297.
[25] B.W. Mwakikunga, A. Forbes, E. Sideras-Haddad, C. Arendse, Phys. Stat. Sol. (a) 205 (2008) 150.
[26] R. Fuchs, K.L. Kliewer, Phys. Rev. 150 (1966) 573.
[27] R. Ruppin, R. Englman, Rep. Prog. Phys. 33 (1970) 149.
[28] G. Gouadec, P. Colomban, Prog. Cryst. Growth Charact. Mater. 53 (2007) 1–56.
[29] H-M. Lin, Y-L. Chen, J. Yang, Y-C. Liu, K.-M. Yin, J-J. Kai, F-R. Chen, L-C Chen, Y.-F. Chen, C-C. Chen, Nano Lett. 3 (2003) 537.
[30] R. Gupta, Q. Xiong, G.D. Mahan, P.C. Eklund, Nano Lett. 12 (2003) 1745.
[31] Q. Xiong, G. Chen, H.R. Gutierrez, P.C. Eklund, Appl. Phys. A 85 (2006) 299–305.
[32] Q. Xiong, J. Wang, O. Reese, L.C. Lew Yan Voon, P.C. Eklund, Nano Lett. 4 (2004) 1991.
[33] S. Bhattacharya, A. Datta, S. Dhara, D. Chakravorty, J. Raman Spectrosc. 42 (2011) 429–433.
[34] Q.H. Xiong, R. Gupta, J. Wang, G.D. Mahan, L.C. Lew Yan Voon, P.C. Eklund, Solid State Phenom. 121–123 (2007) 955–966.
[35] A.K. Arora, M. Rajalakshmi, T.R. Ravindran, V. Sivasubramanian, J. Raman Spectrosc. 38 (2007) 604.
[36] A.K. Arora, M. Rajalakshmi, T.R. Ravindran, Encyclopedia of Nanosci & Nanotechnol., 2003, ISBN 1-58883-001-2.
[37] G. Lermann, T.A. Bischop, T.A. Materny, W. Kiefer, Phys. Rev. B 56 (1997) 7469.
[38] Y.K. Kim, H.M. Jang, Solid State Commun. 127 (2003) 433.
[39] K.R. Zhu, M.S. Zhang, Q. Chen, Z. Yin, Phys. Lett. A 340 (2005) 220–227.
[40] B.W. Mwakikunga, A. Forbes, E. Sideras-Haddad, C. Arendse, Nanoscale Res. Lett. 3 (2008) 372.
[41] B.W. Mwakikunga, E. Sideras-Haddad, M. Maaza, Opt. Mater. 29 (2007) 481.
[42] B.W. Mwakikunga, E. Sideras-Haddad, M. Witcomb, C. Arendse, A. Forbes, J. Nanosci. Nanotechnol. 9 (2009) 3286.

Please cite this article in press as: B.W. Mwakikunga, et al., From phonon confinement to phonon splitting in flat single nanostructures: A case of VO_2@V_2O_5 core–shell nano-ribbons, Vib. Spectrosc. (2012), doi:10.1016/j.vibspec.2012.02.007